REPORT DOCUMENTATION PAGE

Form Approved OMB No. 074-0188

1. AGENCY USE ONLY (Leave blank)	2. REPORT DATE	3. REPORT TYPE AND DATES COVERED
	1998	

4. TITLE AND SUBTITLE
Advanced Oxidation and Reduction Processes in the Gas Phase Using Non-Thermal Plasmas

5. FUNDING NUMBERS
N/A

6. AUTHOR(S)
Louis A. Rosocha, Richard A. Korzekwa

7. PERFORMING ORGANIZATION NAME(S) AND ADDRESS(ES)
Los Alamos National Laboratory
PO Box 1663
Los Alamos, NM 87545

8. PERFORMING ORGANIZATION REPORT NUMBER
LA-UR-98-968

9. SPONSORING / MONITORING AGENCY NAME(S) AND ADDRESS(ES)
SERDP
901 North Stuart St. Suite 303
Arlington, VA 22203

10. SPONSORING / MONITORING AGENCY REPORT NUMBER
N/A

11. SUPPLEMENTARY NOTES
Submitted to Journal of Advanced Oxidation Technologies.

12a. DISTRIBUTION / AVAILABILITY STATEMENT
Approved for public release: distribution is unlimited.

12b. DISTRIBUTION CODE
A

13. ABSTRACT ***(Maximum 200 Words)***

In the past several years interest in gas-phase pollution control has increased, arising from a larger body of regulations and greater respect for the environment. Advanced oxidation technologies (AOTs), historically used to treat recalcitrant water pollutants via hydroxyl-radicals (OH), are now being applied to gas-phase pollutants using non-thermal plasmas (NTPs). These plasmas are useful for generating highly reactive species (e.g., free radicals) which readily decompose entrained pollutants in atmospheric-pressure gas streams. Such plasmas can generate both oxidative and reductive radicals - showing promis for treating a wide fvariety of pollutants, in some cases simultaneously decomposing multiple species. In this paper, we will discuss NTPs views as an AOT; that is, a technique for free-radical-initiated pollutant decomposition. Our primary discussion topics are example applications of the tehchnology, representative plasma reactors, reactive species generation, basic decomposition chemistry, simple analytical removal-scaling models, and the results of laboratory experiments and field trails on representative compounds.

14. SUBJECT TERMS
nonthermal plasma; NTP; advanced oxidation technologies; AOTs; SERDP; SERDP Collection

15. NUMBER OF PAGES
52

16. PRICE CODE N/A

17. SECURITY CLASSIFICATION OF REPORT	18. SECURITY CLASSIFICATION OF THIS PAGE	19. SECURITY CLASSIFICATION OF ABSTRACT	20. LIMITATION OF ABSTRACT
unclass.	unclass.	unclass.	UL

LA-UR- 98-968

Approved for public release; distribution is unlimited.

Title: ADVANCED OXIDATION AND REDUCTION PROCESSES IN THE GAS PHASE USING NON-THERMAL PLASMAS

Author(s): Louis A. Rosocha, CST-18
Richard A. Korzekwa, CST-18

Submitted to: Journal of Advanced Oxidation Technologies

Los Alamos
NATIONAL LABORATORY

Advanced Oxidation and Reduction Processes in the Gas Phase Using Non-Thermal Plasmas

Louis A. Rosocha* **and Richard A. Korzekwa**

Los Alamos National Laboratory, MS E525

PO Box 1663, Los Alamos, New Mexico 87545 (USA)

Abstract

In the past several years interest in gas-phase pollution control has increased, arising from a larger body of regulations and greater respect for the environment. Advanced oxidation technologies (AOTs), historically used to treat recalcitrant water pollutants via hydroxyl-radicals (OH), are now being applied to gas-phase pollutants using non-thermal plasmas (NTPs). These plasmas are useful for generating highly reactive species (e.g., free radicals) which readily decompose entrained pollutants in atmospheric-pressure gas streams. Such plasmas can generate both oxidative and reductive radicals - showing promise for treating a wide variety of pollutants, in some cases simultaneously decomposing multiple species. In this paper, we will discuss NTPs viewed as an AOT; that is, a technique for free-radical-initiated pollutant-decomposition. Our primary discussion topics are example applications of the technology, representative plasma reactors, reactive species generation, basic decomposition chemistry, simple analytical removal-scaling models, and the results of laboratory experiments and field trails on representative compounds.

* Author to whom correspondence should be addressed.

Introduction

Background

Historically the field of Advanced Oxidation Technologies (AOTs) has encompassed processes which decompose organic compounds via the hydroxyl radical OH [Glaze et al 1987 (1)]. AOTs were first used in the treatment of water using OH radicals generated from the photolysis of ozone(O_3) or hydrogen peroxide (H_20_2), or the direct combination of O_3, and (H_20_2). In the past decade, the field has been expanded to include processes which involve other free radicals, some of which are reductive rather than oxidative and to the treatment of gaseous as well as aqueous-based effluents. During the past several years, interest in AOTs has grown considerably because of their applications to pollution control and waste treatment. In many cases this interest has been stimulated by a heightened concern over the pollution of our environment and more stringent environmental regulations (e.g., in the U.S, the Clean Air Act Amendments of 1990 and the Clean Water Act). AOTs show particular promise for the treatment of hazardous and toxic pollutants (e.g., volatile hydrocarbons and halocarbons and oxides of nitrogen and sulfur) because the reaction rates of free radicals with many compounds can be orders of magnitude larger than a strong oxidizer like O_3. Highly reactive species, such as free radicals, can be generated with plasmas.

A plasma (in electrical terminology) is an ionized state of matter (sometimes called *the fourth state of matter)* containing electrons and ions. A plasma behaves much like an *electrical gas,* where the individual charged particles which compose the plasma interact collectively with applied and self-generated electromagnetic fields. Plasmas can be created thermally by heating ordinary matter to a temperature greater than about 10,000 C. In such a *thermal plasma,* all the species - electrons, ions, neutral atoms and molecules - are all in thermal equilibrium (i.e., at the same temperature). Considerable heat energy (enthalpy) must be added to the gas to achieve such an equilibrium. In contrast to a thermal plasma, a *non-thermal plasma (NTP)* (also called non-equilibrium plasma) is characterized by electrons which are not in thermal equilibrium with the other gas species. The electrons are *hot* (few to tens of eV temperature), while the ions and neutral gas species are cold (near-ambient temperature). Such plasmas are good sources of highly reactive oxidative and

reductive species, e.g., $O(^3P)$, OH, N, H, NH, CH, O_3, O_2 ($^1\Delta$), and plasma electrons. Because radical-attack reaction rate constants are very large for many chemical species, entrained pollutants are readily decomposed by NTPs. Via these reactive species, one can direct electrical energy into favorable gas chemistry through energetic electrons, rather than using the energy to heat the gas. NTPs are commonly created by an electrical discharge in a gas or the injection of an energetic electron beam into a gas (2). Both methods create secondary plasma electrons, with a distribution of electron energies defined by an average electron energy (or electron temperature).

As exemplified by the generation of ozone in a dielectric barrier discharge by von Siemens (3), reactions of benzene in a corona discharge by Bertholot (4), and the work of Glockler and Lind (5), the initiation of chemical reactions with NTPs has a history of well over a century.

The roots of treating hazardous and/or toxic chemicals with NTPs go back over two decades to military applications for destroying toxic chemical warfare agents with electric discharge reactors and civilian applications for treating flue gases (SO_x and NO_x) from electric power plants and other installations (e.g., steel mills) with electron beams.

The military applications focused on the removal of highly toxic chemical warfare agents from contaminated air streams to produce breathable air streams [Tevault 1993 (6)]. The first published account of the use of NTPs for decomposing chemical warfare agents involved the treatment of the surrogate agents dimethyl methylphosphonate (DMMP) and diisopropyl methylphosphonate (DIMP) with microwave-generated plasmas [Bailin et al. 1975 (7)]. In the next decade, silent electrical discharges (dielectric-barrier discharges) were studied for this application by other researchers and results published on reactor modeling [Mukkavilli 1988 (8)] and on experiments with test compounds such as organophosphates [Clothiaux et al. 1984 (9], methane [Fraser et al. 1985 (10), Tevault 1985 (11], DMMP and trimethyl phosphate [Fraser et al. 1985 (12)], formaldehyde [Neely 1985 (13)], and hydrogen cyanide [Fraser et al. 1986 (14)]. Because the military-directed systems did not demonstrate the ability to produce byproduct-free breathable air, interest in decomposing such chemicals with NTPs waned.

The first civilian applications of NTPs for pollution control were focused on the removal of oxides of nitrogen and sulfur (NO_x, SO_x) with electron-beam reactors. The scrubbing of flue gases with electron-beam systems was initiated in 1970 in Japan by the Ebara Corporation [Frank & Hirano 1993 (15)] and extensively studied during that decade by Japanese scientists [Kawamura et al. 1978 (16)], and, later, by others [Pearson & Ham 1988 (17)]. At least one study on the decomposition of an organic compound (vinyl chloride) was published in the early 1980s by [Slater & Douglas-Hamilton 1981 (18)].

Based on laboratory and small-scale studies of de-SO_x and de-NO_x, pilot plants and larger demonstration facilities were constructed and tested in Japan, the United States, and Germany [Kawamura et al. 1979 (19), (15), Frank et al 1987 (20), Fuchs et al. 1987 (21), Jordan & Schikarski 1987 (22)]. Chemical models to describe the process in reasonable agreement with experiments were first published by [Tokunaga et al. 1984 (23) and Busi et al. 1985 (24)] and [Matzing 1991 (25)]. Unfortunately, for the early scale-up demonstrations, a lack of commercial acceptance and unfavorable economics compared to conventional systems contributed to a loss of interest in the technology. This interest seems to have been renewed recently, as evidenced by the construction and operation of large-scale facilities in Europe [Chmielewski et al. 1995 (26)].

The removal of SO_x and NO_x from gaseous media was also investigated at laboratory scale using electrical-discharge reactors (pulsed corona) in the 1980s - with pioneering experimental work performed for NO_x by [Masuda & Nakao 1990 (27)] and for SO_x by [Mizuno et al. 1986 (28)]; and modeling work performed by [Gallimberti 1988 (29)]. Following these basic investigations, scale-up of the pulsed corona process for flue gases emitted from a coal-burning electrical power plant was carried out at pilot-plant and demonstration levels [Dinelli et al. 1990 (30), Civitano et al 1993 (31)].

In the late 1980s and early 1990s, further interest in NTP technology for destroying chemical pollutants arose from greater concerns about toxic substances entering and spreading through the environment and the need to meet increasingly-stringent regulations on pollution. The initial work on the destruction of nerve gases and flue gas cleanup has expanded to include many hydrocarbon

and halocarbon compounds in addition to SO_x/NO_x, typically at the laboratory and small pilot-scale levels using pulsed corona [Chang, J.-S. et al. 1991 (32), Grothaus et al. 1993 (33); (2); Penetrante et al. 1995 (34); Lowke & Morrow 1995 (35); Korzekwa et al. 1997 (36); Puchkarev and Gundersen 1997 (37], silent discharges [Chang, M.B. et al. 1991 (38); Storch & Kushner 1993 (39); Sardja & Dhali 1990 (40); Rosocha et al. 1993 (41); Rosocha 1997 (42); Coogan et al. 1993 43)], electrified packed-beds [Virden et al. 1992 (44); Nunez et al.1993 (45)], and electron beams [(17); Paur 1993 (46); (25); Penetrante et al. 1995 (47); Bromberg et al. 1993 (48); Koch et al. 1993 (49); Matthews et al. 1993 (50); Vitale et al. 1996 (51)].

This paper is intended to serve as an overview of the subject of pollutant decomposition in NTPs. We will discuss NTPs in the context of an AOT - namely a tool for free-radical-initiated decomposition reactions. The main points covered are example applications and expected advantages of the technology, representative plasma-chemical reactors, the generation of free radical species, simple analytical models for decomposition-scaling relationships, and the results of selected laboratory experiments and field trails, which illustrate specific energy requirements for the decomposition of example pollutants. Our emphasis is on electric-discharge driven NTP reactors; electron-beam reactors are briefly discussed but the reader is referred elsewhere for more details on that subject [(2); (25); (46); (49); (51); Cohn 1997 (52); Genuario 1997 (53)].

Applications and Expected Advantages

NTP pollution-control is an emerging technology - very few, if any, commercial devices exist at present. But, because promising results, such as the near-complete decomposition of hydrocarbons and halocarbons and the removal of NO_x/SO_x form flue gases, have been obtained in several laboratories and pilot-scale tests, NTP reactors are being considered as viable alternatives for treating industrial-process off-gas streams, stack-gases from primary treatment units (e.g., incinerators), or solvents/volatile chemicals in soil or groundwater. In treating chemicals in soil or groundwater, the chemicals must be transferred to the vapor phase, a step usually accomplished by a vacuum pump or a vacuum-sparger system. Heterogeneous wastes (e.g., solvent-contaminated solids) can also be treated by applying heat to volatilize the solvents and then flushing them out

with an inert carrier gas (e.g., Ar or N_2). NTP pollution control processes are expected to have these distinct advantages over conventional technologies:

- NTP treatment does not produce incinerator by-products such as dioxins and furans;
- NTP operates at near-ambient pressures and temperatures;
- No fuel is added to the process, which minimizes secondary wastes;
- NTP can simultaneously remove hazardous organics and SO_x/NO_x effluents;
- Feedback and automation potential are inherent features of the process;
- No precious, poisonous, or proprietary compounds (e.g., catalysts) are used.

Representative Non-Thermal Plasma Reactors

Figure 1 shows example NTP reactors for gas-phase pollutant processing [(2); Masuda 1988 (54); Mizuno & Ito 1987 (55); (17); (41, 42)]. In an electrical discharge, a high voltage is applied across electrodes in the gas or along a surface adjacent to the gas. An electron-beam reactor requires an electron accelerator to produce the energetic electron beam (~ 100 keV - 1 MeV) that is injected into the process gas. The energetic plasma electrons are responsible for pollutant decomposition, either through direct electron collisions or indirectly through the creation of free radicals that attack the pollutants.

INSERT FIGURE 1 NEAR HERE

The three electric-discharge reactors - silent discharge (dielectric barrier), pulsed corona, and electrified packed bed all create transient electrical-discharge streamers in the gas. The streamer is the source of energetic electrons and other active species. A relatively high voltage (determined by the reactor geometry, gas composition, gas pressure, and gas temperature) is required to cause electrical breakdown in the gas. The necessary voltage is supplied by a drive circuit connected to the reactor. In corona, a non-homogeneous electric field is used to stabilize the discharge and prevent thermal arc formation. Silent discharges use charge buildup on a capacitive barrier to achieve a similar end result. An electrified packed bed is closely related to a barrier discharge.

Another, similar but not illustrated, discharge reactor uses streamers across a dielectric surface. Streamers can be thought of as cylindrical current filaments with typical radius ~ 100 μm. They are transient discharges (e.g., lasting only a few nanoseconds for oxygen or air), fed by ionization and detachment and then arrested when the electric field is reduced to the point where electron attachment becomes dominant. For streamers in pure oxygen and air, the average electron energy and electron density are T_e ~ 3-5 eV, [e] ~ $10^{14}/cm^3$, while a typical breakdown reduced electric field strength in the gas is E/N ~ 100 - 200 Td. Multiple streamers typically give accumulated plasma energy loadings of 10s - 1,000s J/liter atm.

In an electron-beam reactor, the source of electrons (the cathode) can be separate from the accelerating-field section (as in thermionic-cathode and plasma-cathode devices) or integrated with the accelerating-field section (as in a field-emission-cathode electron gun). Electron-beam reactors must use a foil or window to separate the vacuum section of the accelerator from the process gas. The electron beam penetrates the foil, depositing energy in the process gas by collisions and molecular excitation processes coupled to the creation of a large-volume non-thermal plasma. For typical electron-beam reactors, the mean electron energies can be much larger than those for discharge reactors (e.g., ~ 10s eV for electron-beam, as compared to ~ few eV for discharges).

Similar energy loadings can usually be obtained in both electrical discharge and electron-beam reactors (but not necessarily at the same gas flow rates or residence times). For example, typical energy loadings for electron-beam and silent discharge reactors can easily be of order 1 kJ/liter at the same residence time, but considerably lower for a pulsed corona reactor (because the limited number of streamers per unit length that are normally generated).

Active Species Generation and Pollutant Decomposition

In the decomposition process, plasma physics and plasma chemistry are interconnected. The electrical discharge or electron beam creates the plasma which, in turn, generates active species in the pollutant-containing gas. The active species then react with and decompose the chemical pollutants. Below, for an air-like gas, we briefly discuss active species (i.e., radical) generation and

the decomposition chemistry for two example pollutant classes: the flue gas nitric oxide (NO) and the chlorocarbons trichloroethylene (C_2HCl_3, abbreviated TCE) and carbon tetrachloride (CCl_4).

Active Species (Free-Radical) Production

Active species can be formed in a variety of ways in non-thermal plasmas. Table 1 shows the main processes for an air-like carrier gas. Ammonia (NH_3) is also included in the example because it is sometimes employed as an additive in flue-gas processing.

INSERT TABLE 1 HERE

In chlorine-compound-containing mixtures, Cl and ClO radicals are also produced from reactions of radicals and other gas species with the entrained pollutants. These can further participate in decomposition chain reactions.

The yield of a particular radical species (i.e., the number of radicals produced per unit deposited plasma energy) will depend on factors such as the gas composition, the gas pressure, and the average electron temperature. Consider humid, atmospheric pressure air; here the yields of $O(^3P)$, OH, and N radicals in typical electric-discharge reactors are of order 10, 1, and 1 per 100 eV of deposited energy, respectively (41,42). For electron-beam reactors, the $O(^3P)$ yield is about one-third less, the yield of OH is roughly twice as large, and the yield of N is nearly 10 times larger than in discharge reactors (2,47). Another way of stating this difference is that discharge reactors are very efficient producers of oxygen atoms, while electron-beam reactors are very efficient producers of hydroxyl radicals and nitrogen atoms. This means that oxidation reactions with O-atoms have the highest efficiency in discharges, while electron beams can more efficiently promote N-atom-driven reductive reactions in addition to OH-radical-driven oxidation reactions. Usually, pollutants in the concentration range of interest (100s to 1000s ppm) do not affect the electron distribution function or the associated electron temperatures and radical yields.

Basic Decomposition Chemistry

The plasma-generated active species (radicals and secondary electrons) are the initiators of pollutant decomposition reactions. Two major decomposition channels for a gas-phase chemical pollutant X are direct electron impact or chemical (radical-promoted) attack:

$$e + X \rightarrow \text{products}$$

$$O, OH + X \rightarrow \text{products.}$$

The first path is expected to dominate at large contaminant concentrations (when a higher energy fraction is absorbed by the pollutant), while the second should dominate at smaller concentrations. Additionally, some molecules may decompose by ion-molecule reactions as demonstrated by [Penetrante et al. 1997 (56)] for the dissociative charge exchange decomposition of methanol

$$N_2^+ + CH_3OH \rightarrow CH_3^+ + OH + N_2$$

and also postulated by [Krasnoperov et al 1997 (57)] for other hydrocarbons.

The decomposition chemistry for NO is tractable and largely described as follows [2,23,24]:

$$O + NO + M \rightarrow NO_2 + M$$

$$OH + NO_2 + M \rightarrow HNO_3 + M$$

$$O + NO_2 \rightarrow NO + O_2$$

$$N + NO \rightarrow N_2 + O$$

$$N + NO_2 \rightarrow N_2O + O\,.$$

Oxidative-mode reactions involving O-atoms can trap total NO_x as NO and NO_2. Oxidative-mode reactions involving OH-radicals produce nitric acid HNO_3, which can be easily removed by a caustic scrubber. Reductive-mode reactions involving N-atoms instead drive more NO_x to N_2 and O_2 but require higher energy electrons. SO_x removal (38,40) is similarly driven by O-atom and OH-radical oxidative reactions, producing easily-neutralized sulfuric acid as a terminal product.

Ammonia addition is sometimes used to produce other useful products such as ammonium nitrate or ammonium sulfate (agricultural fertilizers).

Other molecules, like many VOCs, will often undergo a series of more complicated reactions before the final products result. The decomposition of a chlorocarbon like trichloroethylene is dominated by free-radical reactions at the relatively high E/N of electric discharges [Evans et al 1993 (58); Falkenstein 1997 (59)].

$$O(^3P) \text{ or } OH + C_2HCl_3 \rightarrow CO_2 + HCl + Cl_2 + COCl_2 + \ldots.$$

Strong electron attachers (e.g.,CCl_4) are preferentially decomposed by dissociative electron attachment at low E/N [(47), Storch et al. 1991 (60)]

$$e + CCl_4 \rightarrow CCl_3 + Cl^-$$

$$CCl_3 + O_2 \rightarrow COCl_2 + Cl + ClO\,.$$

Decomposition is not necessarily complete treatment - the goal is to produce less-toxic or more easily-managed final products. Byproducts must also be considered (e.g., $COCl_2$ is toxic but is easily removed by reactions with water). In laboratory studies, the degree of decomposition and treatment byproducts are measured with an instrument like a gas chromatograph - mass spectrometer.

The detailed plasma-initiated removal chemistry of a particular compound or mixture of compounds can be quite complicated and will not be addressed here. For more information, the reader is referred to the literature. However, to provide some examples that provide some insight into the removal processes, simplified schematic illustrations of TCE and CCl_4 decomposition are shown in Figures 2 and 3.

INSERT FIGURES 2 AND 3 NEAR HERE

Example Decomposition Plots

In many non-thermal plasma devices (like gas lasers, ozonizers, etc.,), a key process parameter is the specific energy (plasma energy density) deposited in the gas. This is also true for the decomposition of a pollutant in an NTP reactor. Experiments with various reactors have shown that the degree of removal of a particular contaminant depends on the applied plasma energy density $\bar{E}$ and a characteristic energy-density parameter (which we call β) which is related to the target compound, the carrier gas, and the reduced electric field E/N for the reactor (2,42,47). The energy density is usually expressed in J/standard liter.

Generally, the degree of removal of a particular contaminant species can be expressed as an exponential function of the parameters $\bar{E}$ and β

$$[X] = [X]_0 \exp(-\bar{E}/\beta) \qquad (1)$$

Such a relationship is representative of chemical-kinetic rate equations that are first order in the concentration of the contaminant. In the next section, we will show that simple, first-order kinetics models can be used to derive a pollutant-removal function whose form is representative of example decomposition plots taken from the literature and shown in Figures 4a-d.

INSERT FIGURES 4a-4d NEAR HERE

Decomposition-Scaling Relationships

Simplified Kinetics Model and Removal Equations

Recent work on comparing different aqueous-phase AOTs has shown that, even though the overall decomposition chemistry of a particular chemical species can be quite complicated, simple kinetic models can be used to describe the rate of radical-initiated decomposition of a target species

[Bolton et al. 1996 (64)]. Using an analogous method for a gas-phase AOT based on an NTP process, we will describe the decomposition of a pollutant X (in a carrier gas of species A and containing radical scavengers S_i) by the following simple chemical reactions and rate equations:

Chemical Reactions	Rate Equations	
$e + A \rightarrow R\cdot + A'$	$\frac{d[R\cdot]}{dt} = \frac{d[R\cdot]}{d\bar{E}} \cdot \frac{d\bar{E}}{dt} = G\bar{P}$,	(2)
$R\cdot + X \rightarrow$ Products	$\frac{d[X]}{dt} = -k[R\cdot][X]$,	(3)
$R\cdot + S_i \rightarrow$ Products	$\frac{d[R\cdot]}{dt} = -k_{S_i}[R\cdot][S_i]$,	(4)

where [X] is the pollutant concentration, G is the production efficiency for radical species R•, $\bar{P}$ is the plasma power density, k is the radical-pollutant kinetic rate constant, $[S_i]$ is concentration of the i^{th} scavenger, and k_{Si} is the scavenging rate constant for the i^{th} species.

Because the rate of radical-pollutant attack is usually quite fast, it is reasonable to assume that the radical R• is consumed as quickly as it is produced; that is, a steady-state approximation for [R•] holds. Under this steady-state assumption, the net rate of change of R• is zero and can be expressed as

$$\frac{d[R\cdot]}{dt}(net) = G\bar{P} - k[R\cdot][X] - \sum_i k_{S_i}[R\cdot][S_i] = 0 \ . \qquad (5)$$

Solving this equation for the steady-state concentration [R•], inserting it into Equation (2), making the substitution $\bar{P} = d\bar{E}/dt$, and rearranging terms, one obtains the following generalized removal differential equation

$$\frac{k[X]+\sum_i k_{S_i}[S_i]}{k[X]}\,d[X]=-G\,d\bar{E}\ . \tag{6}$$

Integration of this equation with the limits $[X]_0 \rightarrow [X]$ and $0 \rightarrow \bar{E}$ gives the transcendental equation

$$\frac{[X]}{[X]_0}+\frac{\sum_i k_{S_i}[S_i]}{k\,[X]_0}\ln\frac{[X]}{[X]_0}-1=-\frac{G\bar{E}}{[X]_0}. \tag{7}$$

When the degree of removal is low; ie., when $[X]/[X]_0 \cong 1 + \ln ([X]/[X]_0$, the following analytical solution (same as Equation 1) is obtained

$$[X]/\,[X]_0 = \exp\,(-\,\bar{E}/\beta)\ , \tag{8}$$

where

$$\beta=\frac{1}{G}\left([X]_0+\frac{\sum_i k_{S_i}[S_i]}{k}\right)\ . \tag{9}$$

When the rate of radical-pollutant attack k[X] is small compared to the rate of radical scavenging $\Sigma_i\, k_{Si}\, [S_i]$, the β-value and, hence the degree of removal $[X]/\,[X]_0$ shows no dependence on the initial concentration $[X]_0$. Similar relationships for the pollutant removal function and its concentration dependence have been derived for electron-beam reactors by [Slater & Douglas-Hamilton (18) and Vitale et al. (51)], assuming that the scavengers are actually products of the initial radical-attack reaction (radical-inhibitor model); and for an electrified packed-bed reactor by [Tonkyn et al. 1996 (65)], with similar assumptions but also taking active-species scavenging by the reactor substrate into account.

In Equation 8 $\bar{E}$ is the applied specific energy (or plasma power divided by gas flow rate, P/Q), and β is the e-fold energy density. Supplying one β to the reactor reduces the concentration by 1/e, 2β by $1/e^2$, and so on. When the β-value is independent of the initial concentration, a plot of the logarithmic degree of removal $-\ln([X]/[X]_0)$ versus $\bar{E}$, gives a straight line of slope $1/\beta$. For other cases, the plot is not necessarily a straight line, so such a slope-determined β-value is only an approximation. When the β-value shows a stronger dependence on the initial pollutant concentration, the removal plot will consist of a family of curves.

Equation 8 does not necessarily apply in all cases. In general, one must numerically solve Equation 7 to obtain the actual removal functions. When the degree of removal is high, the removal plots can show considerable curvature, as observed by [Slater & Douglas-Hamilton (18) and Vitale et al. (51)].

The β-value links the generation of radicals through gaseous electronics/plasma chemistry (G-values) with their utilization through the decomposition chemistry. The G-value is a function of an effective rate constant for radical generation k_{rad} (e.g., the dissociation rate constant for dissociating O_2 molecules into O-atoms), the electron drift velocity v_d, and the reduced electric field strength E/N

$$G = f\left(\frac{k_{rad}}{v_d \frac{E}{N}}\right). \qquad (10)$$

The rate constant k_{rad} and the drift velocity v_d also depend on the reduced field E/N (electron temperature), so the β-value essentially depends on E/N and the chemical kinetics (41, 42).

To show how this simple model predicts the form of the removal equation (as observed in the example decomposition plots presented earlier), we illustrate two examples below. In the first example, the rate of radical scavenging is much greater than the rate of radical attack; i.e., $k[X]_0 << \Sigma_i k_{Si}[S_i]$. In the second example, the opposite situation holds; i.e., $k[X]_0 >> \Sigma_i k_{Si}[S_i]$. Figures 5a,

b show the removal plots which correspond to these two examples for representative values of the initial concentrations and specific plasma energies.

INSERT FIGURES 5a & 5b NEAR HERE

Representative Laboratory Experiments on Pollutant Decomposition

At Los Alamos, we have carried out experiments on the decomposition of several hydrocarbons, halocarbons, and nitric oxide using pulsed corona and dielectric-barrier discharges. In this section, we will discuss tests on two representative VOCs, namely TCE and methyl ethyl-ketone (MEK) in dry air and the flue gas NO in nitrogen and dry air. Other laboratory-scale experiments related to our work at Los Alamos are discussed or referenced elsewhere [Rosocha et al. (41,42); Korzekwa et al. (36); Coogan et al. (43); Falkenstein (59); Coogan & Jassal 1997 (67)].

Description of Apparatus and Experimental Methods

The pulsed corona reactor tube was constructed using a stainless steel corona wire with a diameter of 500 mm and stainless steel tubing with an inner diameter of 2.5 cm as the outer conductor. The length of the tube was 90 cm. A high-voltage alumina feedthrough was employed at one end to apply the electrical pulse to the wire and another alumina insulator was used to support the oppositer end of the wire. The gas flow was introduced into the tube through gas fittings at the gas manifolds on each end. This reactor design could be used up to temperatures of 700 C.

An electrical schematic diagram of the pulsed corona apparatus is shown in Fig. 6. A constant current power supply (EMI model 500-40KV-POS) is used to repetitively charge a storage capacitor, C_{sp}, with a repetition frequency set by the control module. When the breakdown voltage of the coaxial, self-breaking, hydrogen-filled spark gap is reached, a high voltage pulse is delivered to the reactor tube capacitance, C_{pcr}, through the stray inductance, L_s. When the corona inception voltage is reached in the reactor tube, multiple simultaneous streamer-discharges (represented by a time varying resistance R_d) are produced in the tube.

INSERT FIGURE 6 NEAR HERE

A coaxial capacitive voltage divider, V_{pcr}, was constructed at the input to the tube. The voltage probe had a sensitivity of 2.5×10^{-4} V/V and was capable of measuring nanosecond rise time pulses with pulse widths less than 150 ns. The pulsed corona current was measured using a current viewing resistor, R_{cvr}, which was also connected at the reactor input. This probe was capable of measuring nanosecond rise time pulses with a sensitivity of 20 A/V. The power dissipated in the discharge was measured using these probes. A feedback signal from the current probe (signal to indicate the switching of the spark gap) was sent to the control module to inhibit the power supply. For $C_{sp} = 126$ pF, $L_s = 400$ nH, and $C_{pcr} = 25$ pF, the waveforms in Fig. 7 were obtained showing the voltage and current of a typical corona pulse in dry air at room temperature. The energy per pulse E_0 dissipated in the discharge was approximately 60 mJ. $\bar{E}$ is then calculated using the expression $\bar{E} = E_0 f_r / Q$, where f_r is the pulse repetition frequency and Q is the gas flow rate in l/s. The system could be operated at a repetition frequency greater than 1 kHz with a peak output voltage of up to 30 kV.

INSERT FIGURE 7 NEAR HERE

A schematic diagram of the ac-driven dielectric-barrier discharge system is shown in Fig. 8. A variable frequency, 3-kW, ac power supply (Elgar model 3001-165A) was used to drive a high-voltage 50:1 step up transformer (Stangenes Model SI-8020) which supplied power to the dielectric-barrier discharge cell. The operating frequency was 1.2 kHz, with variable discharge powers up to 350 W. The discharge cell was constructed in a flat-plate geometry using two 0.3 cm x 38 cm x 70 cm Pyrex plates with a gap spacing of 3.5 mm and an active discharge area of 1800 cm^2. Two aluminum electrode plates were pressed to each side of the cell. A charge measuring capacitor, C_Q, was placed in the circuit between the low voltage plate and ground. The charge through the cell is proportional to the voltage measured across C_Q (Q_{CELL} in Figure 8). The output of the high-voltage transformer was connected to ground and the high-voltage electrode plate. A high-voltage probe (Tektronix model P6015A) was used to measure the voltage across the cell, V_{CELL}. Typical waveforms of the voltage and charge versus time are shown in Figure 9a. Using the method

invented by [Manely 1943 (68)], the energy per cycle delivered to the discharge was obtained by plotting the charge driven through the cell versus the voltage across the cell for one cycle then calculating the area of the resulting parallelogram, shown in Figure 9b. The power dissipated in the discharge, in Watts P, was then found by multiplying the energy per cycle by the operating frequency. The energy density is computed using the relationship $\bar{E} = P/Q$.

INSERT FIGURES 8 & 9 NEAR HERE

The chemical diagnostics setup is shown in Fig. 10. For the TCE and MEK measurements, a gas bottle was filled to a high pressure with a mixture of dry air and the desired VOC concentration. A mass flow controller was used to set the flow through the discharge tube or cell before entering the vent. Two methods were used to measure the decrease in VOC concentration, 1) a gas-chromatograph/mass-spectrometer, GC/MS, (HP model 5890 GC and HP model 5972 MS) was connected directly to the output line of the discharge volume and 2) a gas-tight syringe was used to extract a sample at a known volume from the gas output line which was then injected into a gas chromatograph with a sample concentrator (Varian model Star 3400CX GC and OI Corp. model 4460A sample concentrator). The data for the ac-driven dielectric-barrier discharge was obtained using the GC/MS and the data for the pulsed corona discharge was obtained using the GC with a sample concentrator. For the measurements of NO in nitrogen and dry air, a cylinder of 2000 ppm NO in nitrogen was mixed down to 200 ppm of NO using either nitrogen or dry air in a separate higher capacity cylinder and two mass flow controllers. The resulting flow was then fed into the reactor. This method of producing the final NO concentration was especially important when using dry air, since (in the presence of oxygen) NO will be converted to NO_2 over an extended period of time. A chemiluminescent detector was used to measure the NO and NO_2 concentration at the output of the reactor, where a 3-m length of 0.6-cm diameter Teflon tubing was used to connect the reactor to the detector through a metal bellows pump.

INSERT FIGURE 10 NEAR HERE

Experimental Results

The removal of two VOCs, TCE and MEK, in dry air and the flue-gas NO in nitrogen or dry air has been measured using the two different discharge reactors. The removal fraction is defined as $[X]/[X]_o$, where $[X]_o$ is the initial concentration and [X] is the final concentration in units of ppmv. The removal fraction (or degree of removal) is plotted as a function of plasma energy deposited into the gas or specific energy, $\bar{E}$.

The first measurements were made using the VOCs to compare the pulsed corona and ac-driven dielectric-barrier discharges at room temperature. Figure 11 shows the removal fraction versus $\bar{E}$ for 200 ppm of TCE, where there is no noticeable difference in the removal efficiency for energy densities up to 400 J/l between these two types of discharges. A double-exponential curve fit is also plotted which shows a slight divergence from a single-exponential fit (a straight line), likely indicating reactions other than first order at the higher energy densities. A double-exponential curve fit applies to all of the removal data presented with the exception of NO in dry air. A similar plot for 1000 ppm of MEK is shown in Fig. 12, where for energy densities up to 1500 J/l, there is no distinguishable difference in the degree of removal. However, for higher energy densities there is a slight difference which can be attributed to a difference in gas temperature which will be discussed in the next section.

INSERT FIGURES 11 & 12 NEAR HERE

Depending on the compound to be treated and the reaction chemistry, the removal fraction can be greatly affected by temperature. The temperature dependence of the reaction kinetics has the form $k = A \exp(-T_A/T)$, where k is the rate constant in units of cm^3/molecule-s, A is the pre-exponential factor with the same units as k, and T_A is the activation energy in units of temperature (K). For reactions with $O(^3P)$, the values of T_A are1000 K and 1300 K for TCE and MEK respectively [Westley et al. 1994 (69), Ott et al. 1995 (70)]. In order to achieve the high energy densities in Figure 12, the pulsed corona tube was operated at powers up to 30 W, which resulted in a temperature increase of up to 60 C. It is plausible that the slight increase in the removal fraction

of MEK in Fig. 12 at energy densities higher than 1500 J/l is attributed to this increase in gas temperature. A temperature rise was not observed in the measurements for TCE using the pulsed corona discharge because the powers necessary to achieve energy densities up to 400 J/l were very low (a few watts). The temperature in the ac-driven dielectric-barrier discharge always remained near room temperature.

Removal measurements were also made for NO in nitrogen and dry air using both the pulsed corona and ac-driven dielectric-barrier discharges. In Fig. 13, the removal fraction versus energy density for NO in nitrogen is plotted, where $[X]/[X]_o$ is defined as the final concentration over the initial concentration for NO and is also defined as the final NO_2 concentration over the initial NO concentration for NO_2. In this case there is a significant difference between the pulsed corona and dielectric-barrier discharges. The energy density required to achieve one e-fold removal is 40 J/l and 65 J/l for the pulsed corona and dielectric-barrier discharges, respectively. A small amount of NO_2 is produced in the reactor which reaches a peak at low values of $\bar{E}$ and decays slowly at higher values of $\bar{E}$. In nitrogen, NO is predominantly converted to N_2 and O_2 (where reductive chemistry through interactions with N-radicals dominates). At the higher energy densities, the small amount of NO_2 is also converted to N_2 and O_2 via reductive chemical processes. In Fig. 14, the removal fraction versus energy density is plotted for NO in dry air. Again as stated above, the NO_2 removal fraction is referenced to the initial NO concentration. In dry air, the pulsed corona and dielectric-barrier discharges produce the same results. Under these conditions, all of the NO is converted to NO_2 (representing the dominance of oxidative chemistry). As seen in Fig. 14, as the NO concentration decreases, there is a corresponding increase in NO_2, where it takes approximately 30 J/l to achieve one e-fold of NO removal.

INSERT FIGURES 13 & 14 NEAR HERE

Discussion of Results

The breakdown voltage in the pulsed corona discharge is much higher than in a low-frequency ac-driven dielectric barrier discharge. The minimum voltage to produce a discharge in the pulsed

corona tube was 12 kV for this wire and tube size, which, if only the geometry is taken in consideration, produces an electric field of 120 kV/cm at the wire surface. The breakdown voltage in the ac-driven dielectric barrier cell was 7 kV at 1.2 kHz with a 3.5-mm air gap, which gives an electric field of 20 kV/cm. With such a large difference in breakdown electric field, it is reasonable to expect a difference in removal fractions between the ac-driven and pulsed corona discharges. However, as seen in the VOC data, there was no difference in removal fractions between the different types of discharges at room temperature. To explain this, the reaction pathways leading to the destruction of these compounds must be investigated. For TCE and MEK in air it is well known that the initial chemical reaction is with the $O(^3P)$ radical produced in the discharge [Westley et al. (69)]. In that case, the production of $O(^3P)$ as a function of the reduced electric field strength E/N (which is also a measure of the average electron energy in the discharge) is important.

As observed in Equation 10, radical-production G-values depend on E/N. The values of the breakdown E/N derived from the breakdown electric fields calculated above are 80 Td for the ac-driven dielectric-barrier discharge and approximately 500 Td for the pulsed corona discharge at room temperature and pressure. The two possible explanations for the same removal efficiencies at different breakdown fields are:1) the radical production happens to be approximately the same for the 80 Td discharge and the 500 Td discharge ($O(^3P)$-radical production G-values at first rise with increasing E/N and then fall off at higher E/N [Rosocha et al. (41), Rosocha (42); Li et al. 1995 (71)], or 2) the observed removal fractions (which correspond to radical formation efficiencies) suggest equivalent average conditions, where the radical formation depends on an average value of E/N (or electron energy), which may be similar for the low-frequency and pulsed discharges.

The only difference between the two discharges was observed for the case of NO in nitrogen. As stated before, the pulsed corona discharge is inherently different than a low frequency dielectric-barrier discharge (a higher breakdown voltage in the pulsed corona produces a higher E/N at breakdown). An electron energy distribution with a higher mean energy (higher E/N) is capable of producing more N-radicals. The higher breakdown voltage of the pulsed corona coupled with a short pulse duration (~ 20 ns) is a possible explanation for the difference in NO removal in nitrogen between these two devices. In air, as opposed to pure nitrogen, the interaction between NO and O-radicals is now the dominant chemical process producing NO_2 and the final products. Since O-

radical production is predominant at low to moderate electron energies, the small difference in the electron energy distribution between the pulsed corona and dielectric-barrier discharges becomes insignificant.

Representative Field Test of an NTP Processor

At Los Alamos, we have had the opportunity to participate in four field tests of silent discharge plasma processing equipment: two tests on VOCs pulled from the ground using soil vapor extraction (SVE), the first at the U.S. Department of Energy (DOE) Savannah River Site [(Rosocha et al. (66)], the second at the McClellan Air Force Base near Sacramento, California (66); one test on the treatment of low-concentration VOCs (< 10 ppm) sparged from groundwater at the Tinker Air Force Base near Oklahoma City, Oklahoma [Rosocha et al. 1998 (72)]; and a test on the treatment of air emissions from a SEMATECH member-site semiconductor manufacturing facility [Coogan & Jassal (67)]. The pilot-scale, mobile plasma-processing equipment that was used for the McClellan and Tinker tests was designed and constructed for industrially-relevant field tests on toxic air emissions under cooperative agreements with the Electric Power Research Institute (EPRI) and a technology-commercialization partner High Mesa Technologies (HMT). Because the McClellan test was probably the most rigorous in terms of the number of compounds to be treated, its duration, and the plasma power requirements, we have chosen to use it as an example for this paper. Summary descriptions of the equipment, test methods, and the results are presented in this section.

Background

In cooperation with the US Environmental Protection Agency (EPA) and the California EPA, and under the overall supervision of CH2MHill, Inc., the US Air Force sponsored tests of innovative remediation technologies under industrial, real-life conditions. An SDP technology-demonstration proposed by LANL's partner HMT was chosen for a two-month campaign at a test site at McClellan Air Force Base in Sacramento, California. This site had formerly been used as a

disposal facility for a variety of solvents, volatile, and semi-volatile chemicals (perhaps more than 50 compounds are entrained in the ground). A partial list of contaminants at the McClellan test site includes TCE, 1,1,1-TCA, PCE, 1,1,1-dichloroethylene (1,1,1-DCE), benzene, toluene, ethylbenzene, xylenes, Freon 113 (a chloro-fluorocarbon), methylene chloride, vinyl chloride, and acetone.

Description of Equipment and Test Methods

Based upon information and experience gained from the Savannah River field test and technical progress since then, LANL and HMT modified the mobile unit that was developed under the EPRI-LANL agreement for more robust operation and about a three-fold increase in gas flow capacity (i.e., to 10 SCFM or 280 std liter/min). An illustration of the upgraded mobile unit is shown in Figure 15. This unit incorporates two NTP processors, each one consisting of two banks of ten planar SDP cells in a containment tank. Each set of twenty cells is electrically driven by an 18-kW rating sinusoidal-waveform power supply connected through a tuning circuit to a high-voltage step up transformer. The gas flow is fed to the tanks in a parallel configuration. Each tank is usually operated at one-half the total gas flow (5 SCFM or 140 std liter/min) with approximately 10 kW of plasma power. This gives an energy density in excess of 4 kJ/std lit. Gas-sampling ports are located before and after each tank. Heat is generated from the electrical power fed to the SDP cells and is removed with a heat exchanger which uses oil as a working fluid. Gas flows, temperature, pressures, and electrical power are monitored with sensors and the data is stored and analyzed using a computer-based data acquisition and control system.

INSERT FIGURE 15 NEAR HERE

Before going to the McClellan site, laboratory tests were conducted at Los Alamos to determine the destruction efficiency, characterize the destruction products, and determine the plasma operating conditions for some of the major compounds expected in the field. This information was needed to specify the operating-parameter range for the field-demonstration equipment. Surrogate test mixtures contained TCE, TCA, PCE, DCB, toluene, and methylene chloride as principal

components. The compound hardest to decompose was TCA. Unfortunately, it was also the one with the highest expected site concentration. Each species was also easier to treat in dry mixtures than in humid gas mixtures. Fortunately, the other two species with expected high site concentrations, TCE and PCE, showed greater than 1.5 and 1.0 decades DRE (destruction and removal efficiency), respectively, at our selected 4 kJ/std lit field operating condition - even for 100% relative humidity.

At the site, the compounds were vacuum extracted from the ground and a portion of the vapor-laden air stream is directed to the technologies to be tested, while the majority of the stream and the test-technology effluents sent to an existing thermal-catalytic oxidation system. The air stream extracted from the ground contained total VOC concentrations of approximately 300 - 1000 ppmv during these tests.

The test program included extensive analytical sampling and chemical analysis. VOCs, semi-volatile organic compounds, carbon dioxide, carbon monoxide, and oxygen were analyzed in both influent and effluent gas streams to evaluate the treatment effectiveness. The treated gas stream and residues generated from the SDP treatment process were also analyzed for dioxins, furans, hydrochloric acid, nitrogen dioxide, ozone, and phosgene.

Summary Results

At the McClellan site, HMT conducted a series of tests over a period of about two months, with technical assistance from LANL. During this time, the SDP system operated more than 400 hours with a maximum continuous operation time of four days. The system treated gas flows as high as 10.4 SCFM (295 std lit/min) and achieved a total DRE as high as 99.4%. Normally the air stream extracted from the ground had a near-saturated relative humidity (i.e., about 100%). In some cases, the influent gas stream was dried with an in-line dehumidifier before being treated. In agreement with the pre-field laboratory tests, the dry streams achieved higher DREs. For some of the test runs, hydrogen gas, with a concentration approximately matching the total VOC concentration, was injected into the gas stream before the SDP units. This tended to increase the achieved DREs.

Table 2 shows summary total DRE data under different gas conditions, gas temperatures, inlet VOC concentrations, gas flow rates, and plasma energy densities.

INSERT TABLE 2 NEAR HERE

The easiest compounds to remove were TCE, toluene, and PCE. The most difficult compounds to remove were methylene chloride, Freon 113, and 1,1,1-TCA. DREs for these three compounds were often below 90% without hydrogen addition or dehumidification. The best performance was achieved with hydrogen addition and dehumidification. Individual-compound DREs (averaged over samples with dry air and added H_2) are shown in Table 3 (73).

INSERT TABLE 3 NEAR HERE

Hydrochloric acid is an inevitable product in the treatment of chlorinated hydrocarbons and significant amounts of liquid HCl were generated in these tests. This can be easily treated in a wet caustic scrubber/neutralizer attached to the SDP system. Approximately 59-65 ppmv of nitrogen dioxide and 58-59 ppmv of ozone were also detected in the effluent gas stream. Phosgene was not detected. Semivolatile compounds, principally napthalene and 2-methylnapthalene, were detected at combined concentrations ranging from 0.091 ppmv to 2.184 ppmv. Total polychlorinated dibenzodioxin (PCDD) and polychlorinated dibenzofuran (PCDF) emissions were extremely small - measured average emissions of 0.0657 ng/m^3 for the combined tetra-, penta-, hexa-, and hepta-CDD congeners and 0.115 ng/m^3 for the same CDF congeners.

Based on the results of field testing, we are encouraged to continue scale-up and commercialization activities. Some practical engineering issues will need to be addressed but these are considered a normal part of making the transition from an emerging technology to a commercial reality.

Conclusions and Summary

Many hazardous organic chemicals and the flue gases NO_x and SO_x are readily attacked by the free radicals generated in non-thermal plasmas. In general, the degree of removal of a particular chemical species scales exponentially with the plasma energy density. The characteristic e-fold energy density depends on the specific pollutant and the carrier gas composition. The plasma-initiated decomposition chemistry of a particular compound or mixture can be quite complicated and has been the subject of both laboratory and field investigations. NTP treatment is expected to be particularly advantageous for the simultaneous removal of multiple pollutants or for pollutants that are difficult to treat with conventional technologies. It should be emphasized that NTP is an emerging air-emissions control technology. Very few (if any) commercial systems exist. Also, for many emissions applications, the present forms of NTP technology are expected to be energy intensive in terms of the electrical power consumption and may require ancillary equipment (e.g., scrubbers) to handle treatment byproducts. Realizing the performance and economic limitations of stand-alone NTP reactors, some workers in this discipline have proposed the use of staged or hybrid systems to better match particular air-emissions control problems. The stand-alone application is only about a decade old. Therefore, more work is needed to optimize and mature the process for widespread commercial use. Hybrid systems might very well be the way of the future for improving performance, economics, and the match to the emissions stream.

References

(1) Glaze, W.H.; Kang, J.W.; and Chapin, D.H. *Ozone: Science & Engineering* **1987**, 9, 335-352.

(2) Several excellent collections of NTP articles appear in the following sources:

(a) Penetrante, B.M. and Schultheis, S.E., Eds. *Non-Thermal Plasma Techniques for Pollution Control, NATO ASI Series, Vol. G34, Parts A & B;* Springer-Verlag: Berlin & Heidelberg, 1993.

(b) Chang, J.-S. and Ferreira, J.L., Eds. *Proceedings of the Second International Symposium on Non-Thermal Plasma Technology for Gaseous Pollution Control*; Catholic University of Brasilia Press: Brasilia, Brazil, 1998.

(c) Chang, J.-S. and Penetrante, B.M.; Guest Eds. *J. Adv. Oxid. Technol. Special Issue on Non-Thermal Plasma Technologies* **1997**, 2 (part of the proceedings of the Third International Conference on Advanced Oxidation Technologies, Cincinnati, OH, Oct. 26-29, 1996).

(d) *Proceeding of First International EPRI/NSF Symposium on Advanced Oxidation*, EPRI TR-102927-V2; Electric Power Research Institute: Palo Alto, CA, 1993.

(e) *Abstracts, Session Overviews, and Proceedings of 2nd International EPRI/NSF Symposium on Environmental Applications of Advanced Oxidation Technologies*; Electric Power Research Institute: Palo Alto, CA, 1996.

(f) Heberlein, J.V.; Ernie, D.W.; and Roberts, J.T.; Eds. *Proceedings of 12th International Symposium on Plasma Chemistry (ISPC-12)*: University of Minnesota: Minneapolis, MN, 1995.

(3) von Siemens, W. *Poggendorf's Ann. Physik Chemie* **1857**,102, 66.

(4) Bertholot, M. *Compt. Rend.* **1876**, 82, 1357.

(5) Glockler, G. and Lind, S.C. *The Electrochemistry of Gases and Other Dielectrics*; John Wiley and Sons: New York, 1939.

(6) Tevault, D. E. In *Non-Thermal Plasma Techniques for Pollution Control, NATO ASI Series, Vol. G34, Part A;* Penetrante, B.M. and Schultheis, S.E., Eds.; Springer-Verlag: Berlin & Heidelberg, 1993; pp. 49-57.

(7) Bailin, L.J., Sibert, M.E., Jonas, L.A., and Bell, A.T. *Environ. Sci. Technol.* **1975**, 9, 254.

(8) Mukkavilli, S.; Lee; C. K.; Varghese, K., and Tavarides, L. L. *IEEE Trans. Plasma Sci.* **1988**, 16, 652-660.

(9) Clothiaux, E. J.; Koropchack, J. A.; and Moore, R. R. *Plasma Chem. Plasma Process.* **1984**, 4, 15-20.

(10) Fraser, M. E.; Fee, D.A.; and Sheinson, R. S. *Plasma Chem. Plasma Process.* **1985**, 5, 163-173.

(11) Tevault, D. E. *Plasma Chem. Plasma Process.* **1985**, 5, 369.

(12) Fraser, M.E.; Eaton, H.G.; and Sheinson, R.S. *Environ. Sci. Technol.* **1985**, 19, 946-949.

(13) Neely, W.C. "The decomposition of gas phase formaldehyde by plasma discharge," *Proceedings of the 1984 Scientific Conference on Chemical Defense Research*, US Army CRDEC-SP-85006, 1985.

(14) Fraser, M. E.and Sheinson, R. S. *Plasma Chem. Plasma Process.* **1986**, 6, 27-38.

(15) Frank, N.W. and Hirano, S. In *Non-Thermal Plasma Techniques for Pollution Control, NATO ASI Series, Vol. G34, Part B;* Penetrante, B.M. and Schultheis, S.E., Eds.; Springer-Verlag: Berlin & Heidelberg, 1993; pp. 1-26.

(16) Kawamura, K. et al. *J. Atomic Energy Soc. Japan* **1978**, 20, 359-367.

(17) Pearson, J.C. and Ham, D.O. *Radiat. Phys. Chem.* **1988**, 31, 1-8.

(18) Slater, R.C. and Douglas-Hamilton, D.H. *J. Appl. Phys.*, **1981**, 52, 5820-5828.

(19) Kawamura, K. et al. *Radiat. Phys. Chem.* **1979**, 13, 5-12.

(20) Frank, N.W.; Kawamura, K.; and Miller, G.A. In *Electron Beam Processing of Combustion Gases, IAEA-TECDOC-428*; International Atomic Energy Agency: Vienna, 1987; pp. 97-118.

(21) Fuchs, P.; Roth, B.; and Schwing, U. In *Electron Beam Processing of Combustion Gases, IAEA-TECDOC-428*; International Atomic Energy Agency: Vienna, 1987; pp. 119-133.

(22) Jordan, S. and Schikarski, W. In *Electron Beam Processing of Combustion Gases, IAEA-TECDOC-428*; International Atomic Energy Agency: Vienna, 1987; pp. 135-150.

(23) Tokunaga, O.; Mishimura, K.; Machi, S. and Washino, M. *Int. J. Appl. Radiat. Isot.* **1984**, 29, 81-85.

(24) Busi, F.; D'Angelantonio, M.; Mulazzini, G.; Raffaelli, V.; and Tubertini, O. *Radiat. Phys. Chem.* **1985**, 25, 47-55.

(25) Matzing, H. "Chemical Kinetics of Flue Gas Cleaning by Irradiation with Electrons," In *Advances in Chemical Physics, LXXX*; Prigogine, I. and Rice, S.A. Eds.; John Wiley & Sons, Inc.: New York; pp. ???-???.

(26) Chmielewski, A.G.; Iller, E.; Zimek, Z.; Romanowski, M.; and Koperski, K. *Radiat. Phys. Chem.* **1995**, 46, 1063-1066.

(27) Masuda, S. and Nakao, H. *IEEE Trans. Ind. Appl.* **1990**, 26, 374-382.

(28) Mizuno, A.; Clements, J.S.; and Davis, R.H. *IEEE Trans. Ind. Appl.* **1986**, IA-22, 516-521.

(29) Gallimberti, I. *Pure Appl. Chem.* **1988**, 60, 663-674.

(30) Dinelli, G.; Civitano, L.; and Rea, M. *IEEE Trans. Ind. Appl.* **1990**, 26N, 535-541.

(31) Civitano, L. In *Non-Thermal Plasma Techniques for Pollution Control, NATO ASI Series, Vol. G34, Part B;* Penetrante, B.M. and Schultheis, S.E., Eds.; Springer-Verlag: Berlin & Heidelberg, 1993; pp. 103-130.

(32) Chang, J.-S.; Lawless, P.A.; and Yamamoto, T. *IEEE Trans. Plasma Sci.* **1991**, 19, 1152-1166.

(33) Grothaus, M.G.; Hutcherson, R.K.; Korzekwa, R.A.; and Roush, R. *Proceedings of 9th IEEE International Pulsed Power Conference* **1993**, 180-183.

(34) Penetrante, B.M.; Hsiao, M.C.; Merritt, B.T.; and Voghtlin, G.E. *IEEE Trans. Plasma Sci.* **1995,** 23, 679-687.

(35) Lowke, J.J. and Morrow, R. *IEEE Trans. Plasma Sci.* **1995** 23, 661-671.

(36) Korzekwa, R.A.; Rosocha, L.A.; and Flakenstein, Z. *Proceedings of 11th IEEE International Pulsed Power Conference* (Los Alamos National Laboratory Report LA-UR-97-2308, 1997).

(37) Puchkarev, V. and Gundersen, M. *Appl. Phys. Lett.* **1997,** 71, 3364-3366.

(38) Chang, M. B.; Balbach, J. H.; Rood, M. J.; and Kushner, M. J. *J. Appl. Phys.* **1991,** 69, 4409-4417.

(39) Storch, D. G. and Kushner, M. J. *J. Appl. Phys.* **1993**, 73, 51.

(40) Sardja, I. and Dhali, S. *Appl. Phys. Lett.* **1990**, 56, 21-23.

(41) Rosocha, L.A.; Anderson, G.K.; Bechtold, L.A.; Coogan, J.J.; Heck, H.G.; Kang, M.; McCulla, W.H.; Tennant, R.A.; and Wantuck, P.J. In *Non-Thermal Plasma Techniques for Pollution Control, NATO ASI Series, Vol. G34, Part B;* Penetrante, B.M. and Schultheis, S.E., Eds.; Springer-Verlag: Berlin & Heidelberg, 1993; pp. 281-306.

(42) Rosocha, L.A. in *Environmental Aspects in Plasma Science*; Manheimer, W.; Sugiyama, L.E.; and Stix, T.H., Eds., American Institute of Physics Press: Woodbury, NY, 1997; pp. 261-298.

(43) Coogan, J.J.; Rosocha, L.A.; Brower, M.J.; Kang, M.; and Schmidt, C.A. *Proceedings of 11th Ozone World Congress, Ozone in Water and Wastewater Treatment* **1993**, Vol. 2, Section S-15, 25-28.

(44) Virden, J.W.; Heath, W.O.; Goheen, S.C.; Miller, M.C.; Mong, G.M.; and Richardson, R.L. *Proceedings of Spectrum '92 conference, Boise, ID, document PNL-SA-20741*, Pacific Northwest Laboratory (1992).

(45) Nunez, C.M.; Ramsey, G.H.; Ponder, W.H.; Abbott, J.H.; Hamel, L.E.; and Kariher, P.H. *J. Air & Waste Management Assoc.* **1993,** 43, 242-247.

(46) Paur, H.R. In *Non-Thermal Plasma Techniques for Pollution Control, NATO ASI Series, Vol. G34, Part B;* Penetrante, B.M. and Schultheis, S.E., Eds.; Springer-Verlag: Berlin & Heidelberg, 1993; pp. 77-89.

(47) Penetrante, B.M.; Hsiao, M.C.; Bardsley, J.N.; Merritt, B.T.; Vogtlin, G.E.; Wallman, P.H.; Kuthi, A.; Burkhart, C.P.; and Bayless, J.R. *Physics Lett.* **1995,** A209, 69-77.

(48) Bromberg, L.; Cohn, D.R.; Koch, M.; Patrick, R.M.; and Thomas, P. *Phys. Lett. A* **1993,** 173, 293-299.

(49) Koch, M.; Cohn, D.R; Patrick, R.M.; Scheutze, M.P.; Bromberg, L.; Reilly, D.; and Thomas, P. Phys. Lett A **1993,** 184, 109.

(50) Matthews, S.M.; Boegel, A.J.; and Loftis, J.A. *Remediation* **1993**, Autumn, 459-481.

(51) Vitale, S.A.; Hadidi, K.; Cohn, D.R.; and Falkos, P. *Plasma Chem. Plasma Process*. **1996,** 16, 651-668.

(52) Cohn, D.R. in *Environmental Aspects in Plasma Science*; Manheimer, W.: Sugiyama, L.E.; and Stix, T.H., Eds., American Institute of Physics Press: Woodbury, NY, 1997; pp. 209-229.

(53) Genuario, R.D. in *Environmental Aspects in Plasma Science*; Manheimer, W.; Sugiyama, L.E.; and Stix, T.H., Eds., American Institute of Physics Press: Woodbury, NY, 1997; pp. 231-259.

(54) Masuda, S. *Pure Appl. Chem.* **1988** 60, 727-731.

(55) Mizuno, A. and Ito, H. *Proceedings of 3rd Int. Conf. on Electrostatic Precipitators* **1987**, 617-624.

(56) Penetrante, B.M.; Hsiao, M.C.; Bardsley, J.N.; Merritt, B.T.; Vogtlin, G.E.; and Wallman, P.H. *Proceedings of the Second International Symposium on Environmental Applications of Advanced Oxidation Technologies* **1997**, Section 5, 74-88.

(57) Krasnoperov, L.N.; Krishtopa, L.G.; and Bozzelli, J.W. *J. Adv. Oxid. Technol.* **1997**, 2, 248-256.

(58) Evans, D.; Rosocha, L.A.; Anderson, G.K.; Coogan, J.J.; and Kushner, M.J. *J. Appl. Phys.* **1993** 74, 5378-5386.

(59) Falkenstein, Z. *J. Adv. Oxid. Technol.* **1997**, 2, 223-238.

(60) Storch, D.G.; Chang, M.B.; Rood, M.J.; and Kushner, M.J. "Modeling and diagnostics of dielectric barrier discharge destruction of CCl_4," *Unpublished progress report to Los Alamos National Laboratory* (1991).

(61) Helfritch, D.J. In *Non-Thermal Plasma Techniques for Pollution Control, NATO ASI Series, Vol. G34, Part B;* Penetrante, B.M. and Schultheis, S.E., Eds.; Springer-Verlag: Berlin & Heidelberg, 1993; pp. 211-221.

(62) Skalny, J.D.; Sobek, V.; Lukac, P. In *Non-Thermal Plasma Techniques for Pollution Control, NATO ASI Series, Vol. G34, Part A;* Penetrante, B.M. and Schultheis, S.E., Eds.; Springer-Verlag: Berlin & Heidelberg, 1993; pp. 151-165.

(63) Wolf, O. et al, "Experimental Investigations of the Removal of Toxic Exhaust Gas Components by Dielectric Barrier Discharges," *Proceedings of 7th Bundesdeutsche Fachtagung für Plasmatechnologie (BFPT-7)*, **1996**, Poster P 85.

(64) Bolton, J.R.; Bircher, K.G.; Tumas, W.; and Tolman, C.A. *J. Adv. Oxid. Technol.* **1996**, 1, 13-17.

(65) Tonkyn, R.G.; Barlow, S.E.; and Orlando, T.M. J. Appl. Phys. **1996**, 80, 4877-4886.

(66) Rosocha, L.A.; Coogan, J.J.; Korzekwa, R.A.; Secker, D.A.; Reimers, R.F.; Herrmann, P.G.; Chase, P.J.; Gross, M.P.; and Jones, M.R. *Proceedings of the Second International Symposium on Environmental Applications of Advanced Oxidation Technologies* **1997**, Section 5, 107-121.

(67) Coogan, J.J. and Jassal, A.S. "Silent Discharge Plasma (SDP) for Point-of-Use (POU) Abatement of Volatile Organic Compound (VOC) Emissions: Final Report (ESHC003)," *SEMATECH Technology Transfer Document 97023244A-ENG* (1997).

(68) Manley, T. C. *Trans. Electrochem. Soc.* **1943,** 84, 83.

(69) Westley, F.; Herron, J.T.; Hampson, R.F.; and Mallard, W.G., Eds. *NIST Reference Database 17*; National Institute of Standards and Technology: Gaithersburg, MD, 1994.

(70) Ott, P.; Helf, D.; and Kirchner, K. *Dechema-Monographs*, **1995**, 104, 91-98.

(71) Li, J.; Sun, W.; Pashaie, B.; and Dhali, S.K. *IEEE Trans. Plasma Sci.* **1995**, 23, 672.

(72) Rosocha, L.A.; Korzekwa, R.A.; Secker, D.A.; Coogan, J.J.; and Jones, M.R. "Final Report for Joint EPRI-LANL Project: Industrial Air Toxics Treatment Demonstration Using Silent Discharge Plasma," *Los Alamos National Laboratory Report LA-UR-98-700* (1998).

(73) McClellan AFB SERDP Nonthermal Plasma Destruction Technology. http//www.mcclellan.af.mil/EM/TECH/sd_nonth.htm (accessed March 1998).

Table 1: Example Radical Formation Mechanisms.

Electron impact

$e + O_2 \rightarrow O + O^* + e$
$e + N_2 \rightarrow N + N + e$
$e + O_2 \rightarrow O + O + e$
$e + H_2O \rightarrow OH + H + e$
$e + N_2 \rightarrow N_2^* + e$
$e + NH_3 \rightarrow NH + H_2 + e$

Quenching

$O^* + H_2O \rightarrow 2OH$
$N_2^* + O_2 \rightarrow N_2 + O + O$

Ionization/Clusters

$e + O_2 \rightarrow O_2^+ + e$
$O_2^+ + H_2O \rightarrow O_2^+(H_2O)$
$O_2^+(H_2O) + H_2O \rightarrow HO_3^+ + O_2 + OH$
$O_2^+(H_2O) + H_2O \rightarrow HO_3^+(OH) + O_2$
$HO_3^+(OH) + H_2O \rightarrow HO_3^+ + H_2O + OH$

Others

$H + O_3 \rightarrow OH + O_2$
$HO_2 + NO \rightarrow OH + NO_2$
$H + O_2 + M \rightarrow HO_2 + M$

Table 2: Summary results from SDP system tests at McClellan AFB.

Sample Number	Operating Conditions	Gas Temperature (C)	Total Inlet VOCs (ppmv)	Gas Flow (SCFM)	Energy Density (J/std lit)	Total DRE (%)
1	Wet gas/39 cells	32	542	10.0	4162	93.5
2	Wet gas/39 cells	59	462	10.0	4193	88.1
3	Wet gas/39 cells	60	989	9.0	4680	92.5
4	Wet gas/39 cells	58	328	10.0	4185	95.6
5	Wet gas/40 cells	56	333	9.5	4416	90.0
6	Wet gas/40 cells	50	363	10.4	4068	90.0
7	Wet gas/20 cells	20	460	4.7	4494	97.7
8	Wet gas/40 cells	32	493	8.1	4716	92.4
9	Wet gas/15 cells	38	477	5.4	4034	93.0
10	Wet gas/15 cells	38	464	4.1	5075	92.5
11	Wet gas/H_2/15 cells	55	532	4.1	5189	92.5
12	Dry gas/H_2/20 cells	50	629	5.1	4083	99.4
13	Dry gas/H_2/20 cells	18	698	3.7	5734	98.5
14	Wet gas/H_2/20 cells	24	459	2.9	7396	96.7

Table 3 Average individual DREs with added hydrogen and dehumidification (73).

Compound	Avg. Inlet Conc. (ppmv)	Average DRE (%)
TCE	82.7	99.6
PCE	76.3	99.5
1,1,1 TCA	157.0	95.4
Xylenes	16.3	99.4
Acetone	115.6	97.9
TNMOCs*	5515.0	97.0
SVOCs**	0.4744	99.9

*TNMOCs (total non-methane organic compounds)
**SVOCs (semi-volatile organic compounds)

Figure Captions

Figure 1: Schematic diagrams of commonly-employed non-thermal plasma reactors.

Figure 2: Diagram of the dominant reaction pathways for the non-thermal plasma decomposition of TCE, after Evans et al. (58).

Figure 3: Diagram of the dominant reaction pathways for the decomposition of CCl_4 by a non-thermal plasma. Dissociative attachment is the most efficient decomposition initiator for CCl_4 (upper); however, the presence of O-atoms can change the distribution of final products (lower). Reaction schemes after Penetrante et al. (47) and Storch et al. (60).

Figure 4: Representative non-thermal plasma (negative corona and dielectric barrier reactors) decomposition plots taken from the literature. (a) hydrogen sulfide (H_2S) in a H_2/He mixture, after Helfritch (61); (b) CFC-12 (CCl_2F_2) in air, after Skalny (62); (c) TCE in humid air, after Falkenstein (59) and nitric oxide (NO) in flue gas, after Wolf et al. (63); (d) Chlorobenzene (C_6H_5Cl) in synthetic air, after Krasnoperov et al (57).

Figure 5: Example plots derived from the simple radical-initiated-decomposition model, for different initial pollutant concentrations. (a) case for which rate of radical attack dominates rate of radical scavenging; (b) case for which radical scavenging dominates radical attack. Note that for the second case, the decomposition plot is only weakly dependent on initial pollutant concentration and that the dependence increases at higher degrees of removal.

Figure 6: Equivalent-circuit schematic diagram for the pulsed corona reactor apparatus.

Figure 7: Typical measured waveforms for the pulsed-corona reactor voltage and current pulses.

Figure 8: Schematic diagram for the ac-driven dielectric-barrier-discharge apparatus.

Figure 9: Measured voltage and charge for the dielectric-barrier reactor. (a) Waveforms for the voltage across the reactor cell and the charge deposited per cycle on the dielectrics; (b) Charge versus voltage plot for dielectric-barrier reactor measurements (used to determine the plasma energy deposited in the process gas per cycle).

Figure 10: Schematic diagram for the experimental apparatus, including gas mixing station, non-thermal plasma reactor, and gas-analysis instruments.

Figure 11: Decomposition plot for measurements on 200 ppm TCE in dry air, using both pulsed corona and dielectric-barrier reactors.

Figure 12: Decomposition plot for measurements on 1000 ppm MEK in dry air, using both pulsed corona and dielectric-barrier reactors.

Figure 13: Decomposition plots for measurements on 200 ppm NO in pure N_2, using both pulsed corona and dielectric-barrier (silent discharge plasma - SDP) reactors. The normalization of the NO_2 concentration values is described in the text.

Figure 14: Decomposition plots for measurements on 200 ppm NO in dry air, using both pulsed corona and dielectric-barrier (silent discharge plasma - SDP) reactors. The normalization of the NO_2 concentration values is described in the text.

Figure 15: Illustration of the mobile silent discharge plasma processing equipment used in conjunction with soil-vapor extraction for a VOC-treatment demonstration at McClellan Air Force Base (66).

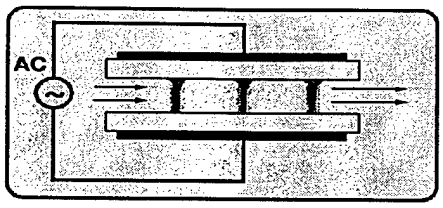

Silent discharge (dielectric-barrier discharge)

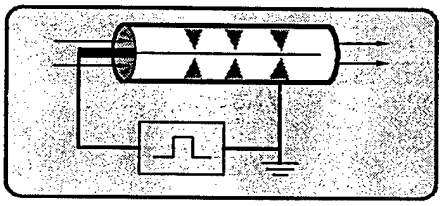

Pulsed or DC corona

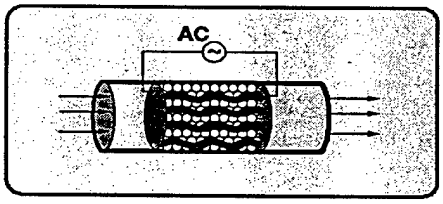

Electrified packed bed

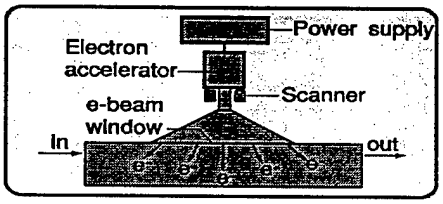

Electron beam

Figure 1

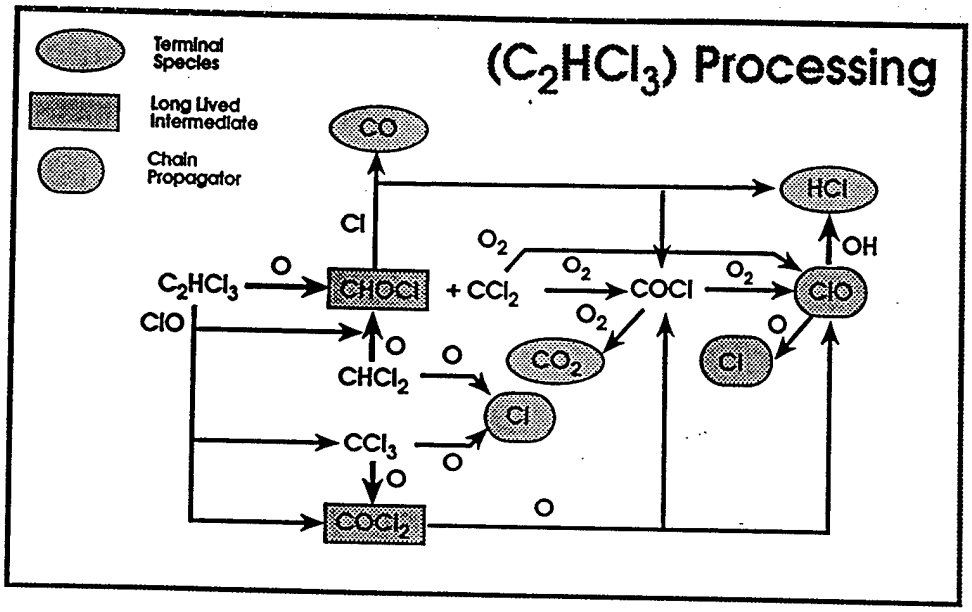
Terminal Species
Long Lived Intermediate
Chain Propagator
(C2HCl3) Processing
CO
HCl
Cl
OH
O2
C2HCl3
O
CHOCl
+ CCl2
COCl
ClO
ClO
O
CHCl2
CO2
Cl
Cl
CCl3
COCl2

Figure 2

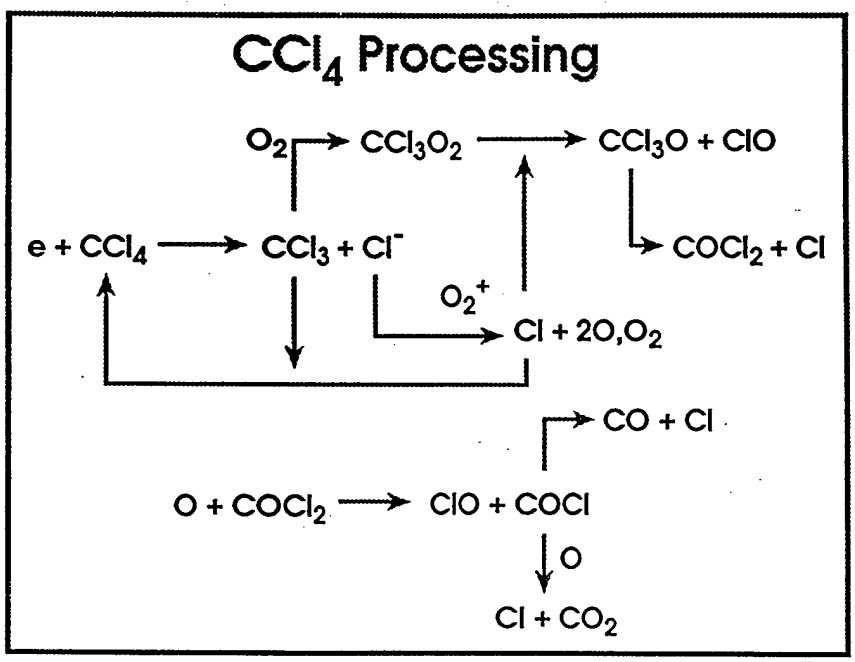
CCl_4 Processing
O_2
CCl_3O_2
$CCl_3O + ClO$
$e + CCl_4$
$CCl_3 + Cl^-$
$COCl_2 + Cl$
O_2^+
$Cl + 2O,O_2$
$CO + Cl$
$O + COCl_2$
$ClO + COCl$
O
$Cl + CO_2$

Figure 3

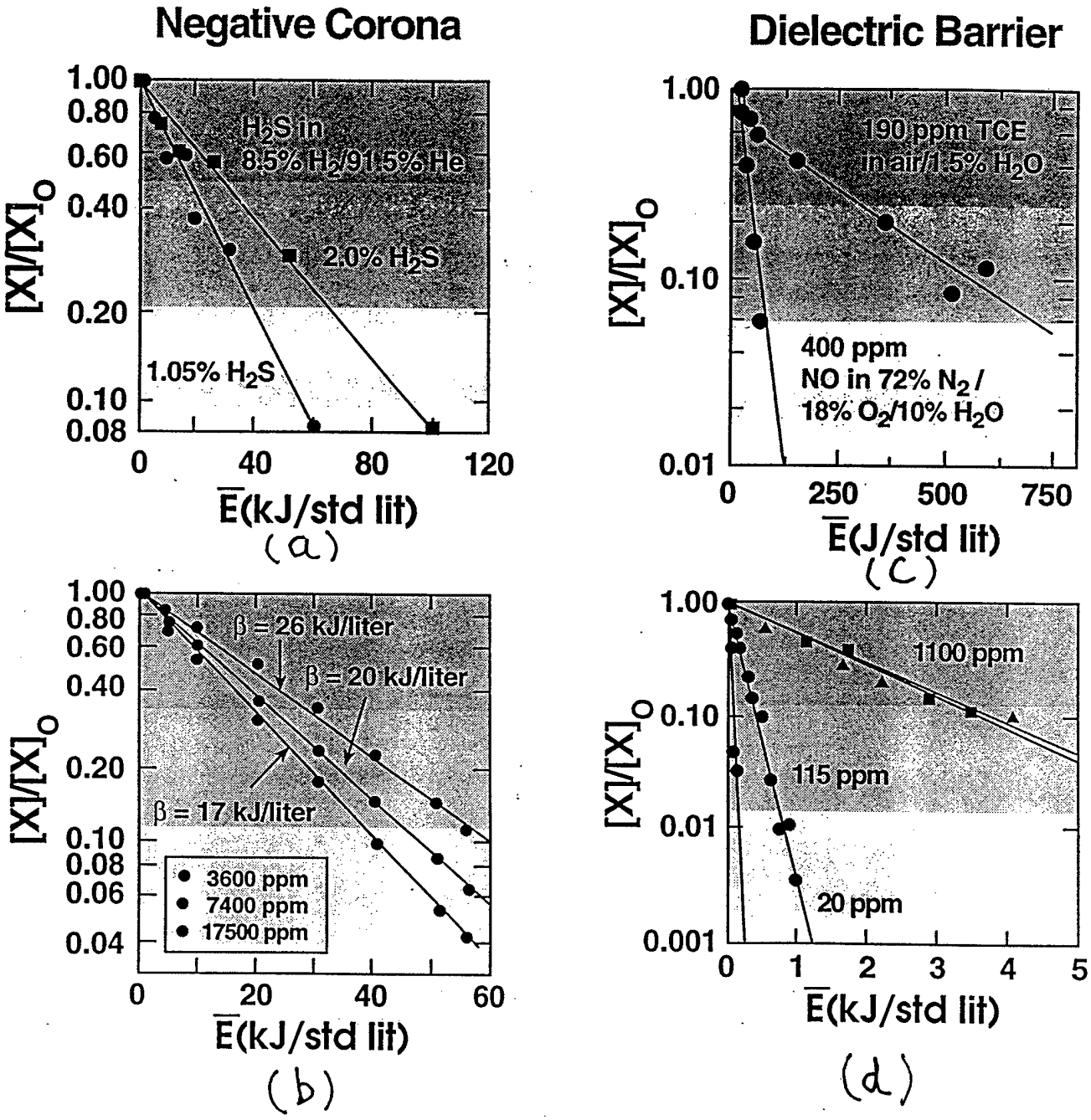
Negative Corona
Dielectric Barrier
1.00
0.80
0.60
0.40
0.20
0.10
0.08
[X]/[X]o
H2S in
8.5% H2/91.5% He
2.0% H2S
1.05% H2S
0
40
80
120
Ē(kJ/std lit)
(a)
190 ppm TCE
in air/1.5% H2O
400 ppm
NO in 72% N2 /
18% O2/10% H2O
0.01
0
250
500
750
Ē(J/std lit)
(c)
β = 26 kJ/liter
β = 20 kJ/liter
β = 17 kJ/liter
0.06
0.04
3600 ppm
7400 ppm
17500 ppm
20
60
Ē(kJ/std lit)
(b)
1100 ppm
115 ppm
20 ppm
0.001
1
2
3
4
5
Ē(kJ/std lit)
(d)

Figure 4

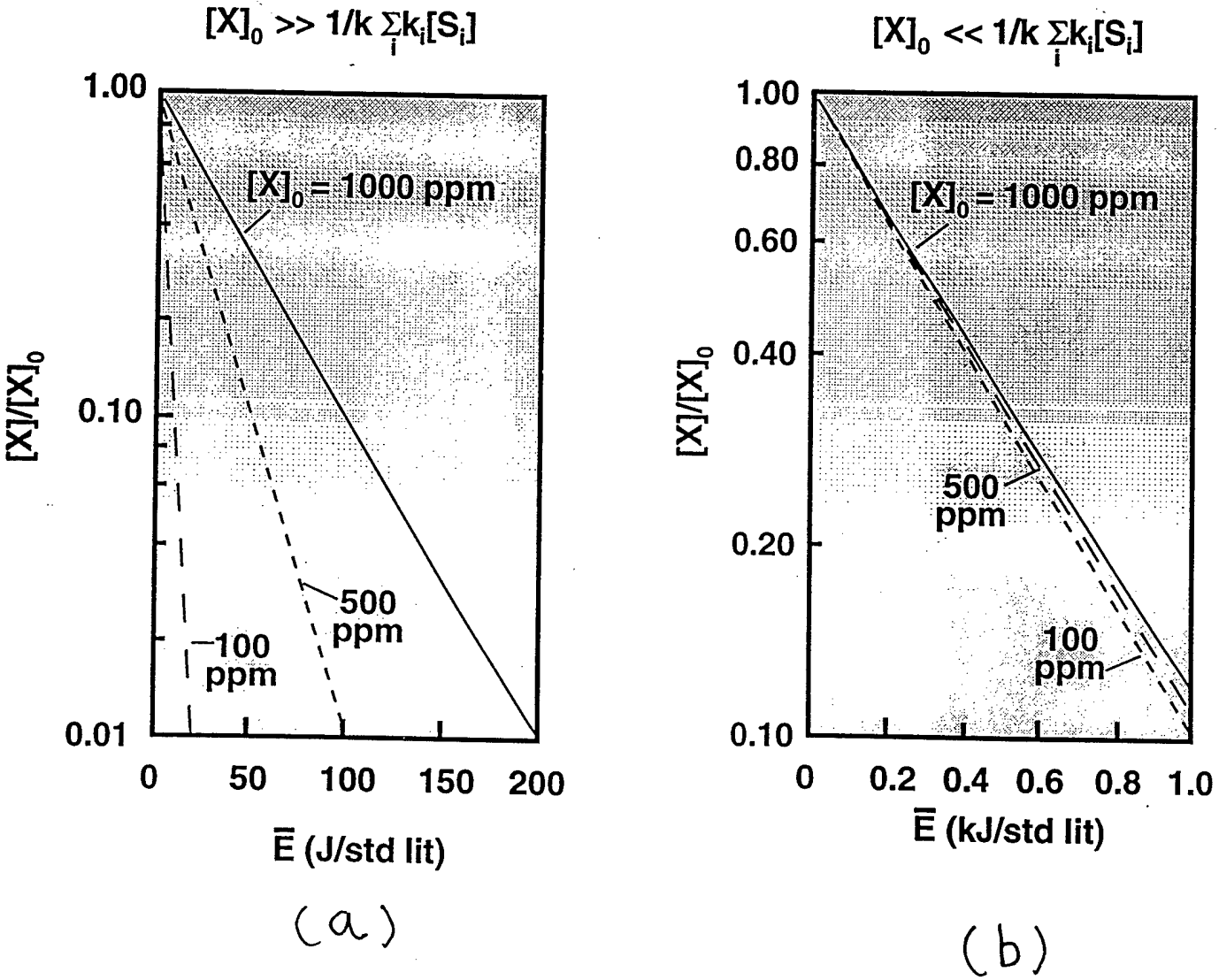
$[X]_0 >> 1/k \sum_i k_i[S_i]$
1.00
0.10
0.01
$[X]/[X]_0$
$[X]_0 = 1000$ ppm
500 ppm
100 ppm
0
50
100
150
200
$\bar{E}$ (J/std lit)
(a)
$[X]_0 << 1/k \sum_i k_i[S_i]$
1.00
0.80
0.60
0.40
0.20
0.10
$[X]/[X]_0$
$[X]_0 = 1000$ ppm
500 ppm
100 ppm
0
0.2
0.4
0.6
0.8
1.0
$\bar{E}$ (kJ/std lit)
(b)

Figure 5

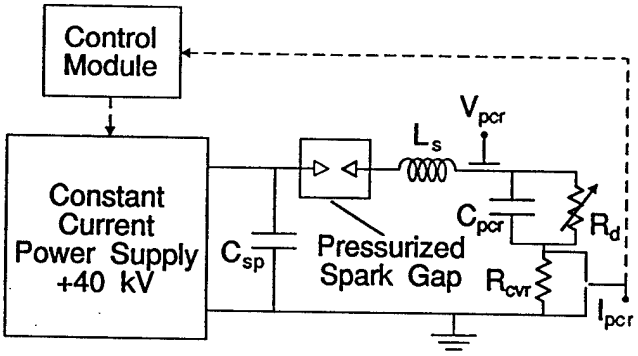
Control Module
Constant Current Power Supply +40 kV
C_{sp}
Pressurized Spark Gap
L_s
V_{pcr}
C_{pcr}
R_d
R_{cvr}
I_{pcr}

Figure 6

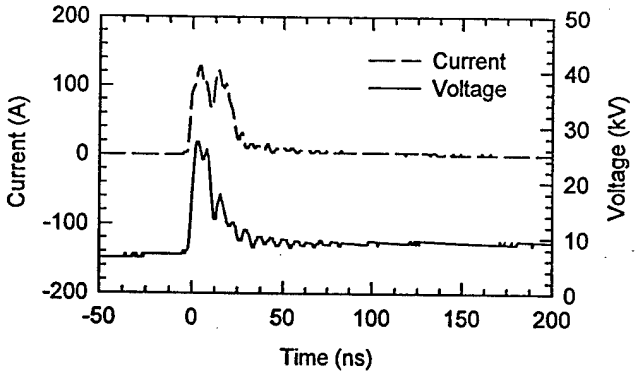
200
100
0
-100
-200
Current (A)
-50
0
50
100
150
200
Time (ns)
50
40
30
20
10
0
Voltage (kV)
Current
Voltage

Figure 7

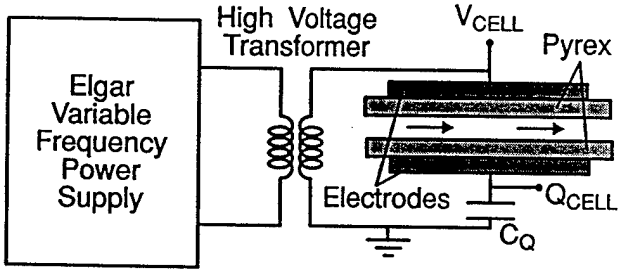
Elgar
Variable
Frequency
Power
Supply
High Voltage
Transformer
V_{CELL}
Pyrex
Electrodes
Q_{CELL}
C_Q

Figure 8

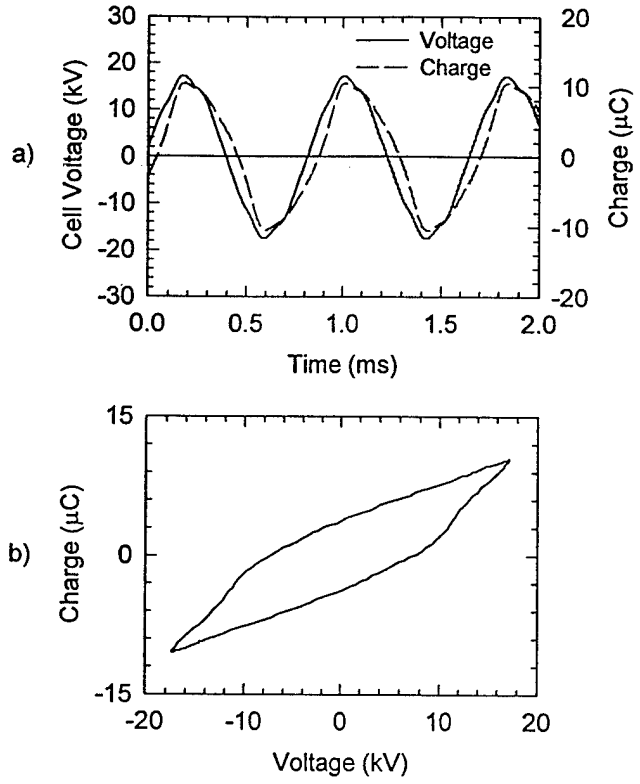
a)
Cell Voltage (kV)
Charge (μC)
Voltage
Charge
Time (ms)
b)
Charge (μC)
Voltage (kV)

Figure 9

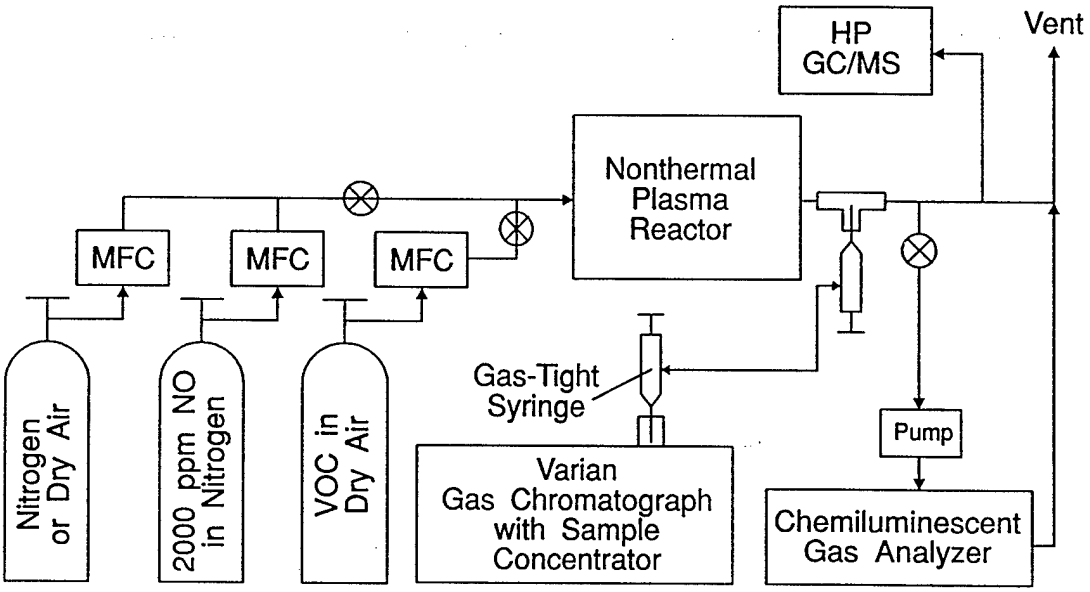
HP
GC/MS
Vent
Nonthermal
Plasma
Reactor
MFC
MFC
MFC
Nitrogen
or Dry Air
2000 ppm NO
in Nitrogen
VOC in
Dry Air
Gas-Tight
Syringe
Pump
Varian
Gas Chromatograph
with Sample
Concentrator
Chemiluminescent
Gas Analyzer

Figure 10

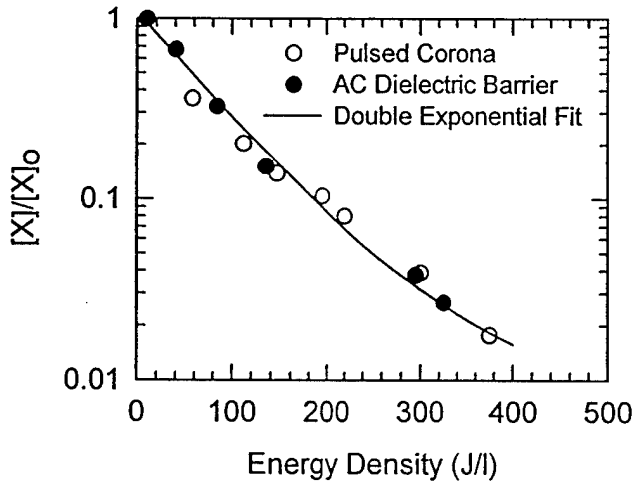
1
0.1
0.01
[X]/[X]o
0
100
200
300
400
500
Energy Density (J/l)
Pulsed Corona
AC Dielectric Barrier
Double Exponential Fit

Figure 11

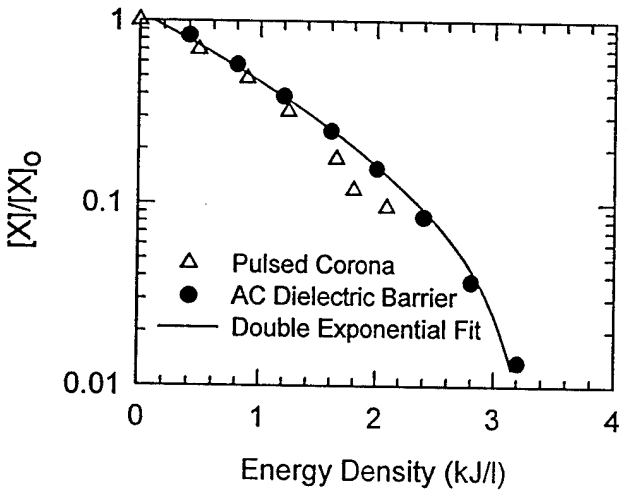
1
0.1
0.01
[X]/[X]o
0
1
2
3
4
Energy Density (kJ/l)
Pulsed Corona
AC Dielectric Barrier
Double Exponential Fit

Figure 12

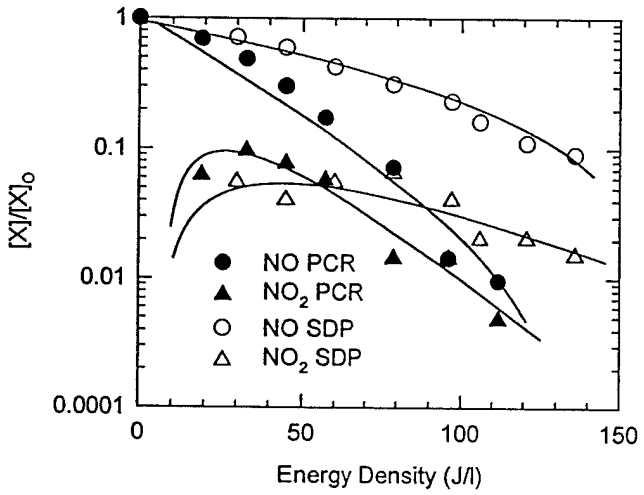
1
0.1
0.01
0.0001
[X]/[X]o
0
50
100
150
Energy Density (J/l)
NO PCR
NO2 PCR
NO SDP
NO2 SDP

Figure 13

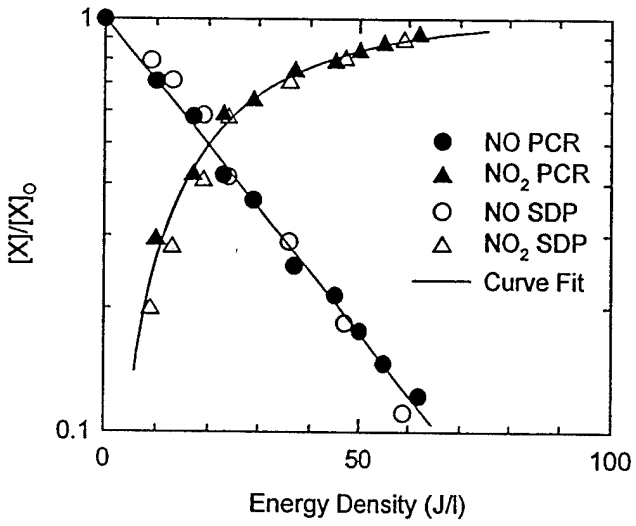
1
0.1
0
50
100
[X]/[X]o
Energy Density (J/l)
NO PCR
NO2 PCR
NO SDP
NO2 SDP
Curve Fit

Figure 14

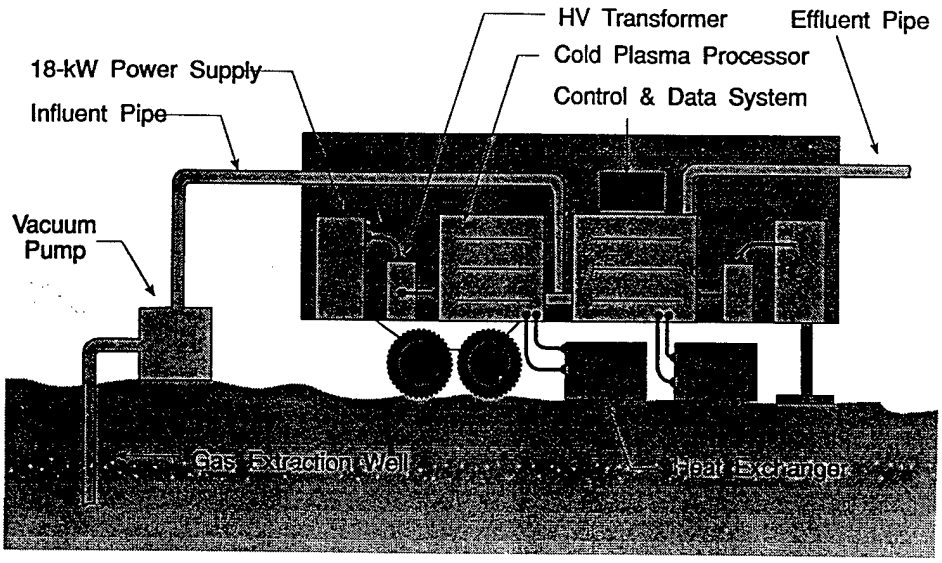
HV Transformer
Effluent Pipe
18-kW Power Supply
Cold Plasma Processor
Control & Data System
Influent Pipe
Vacuum
Pump
Gas Extraction Well
Heat Exchanger

Figure 15